

A COMPARATIVE STUDY OF HELICOPTER ENGINE AIR PARTICLE SEPARATION TECHNOLOGIES

Nicholas Bojdo & Antonio Filippone
 Nicholas.Bojdo@postgrad.manchester.ac.uk
 The University of Manchester
 Manchester M13 9PL
 United Kingdom

Abstract

An investigation into the efficacy of helicopter engine sand filters is conducted. Engine Air Particle Separation devices are broadly split into three categories: Vortex Tube Separators, Integrated Particle Separators, and Inlet Barrier Filters. The first two are inertial separators that scavenge particles by centrifugal force; the latter traps particles on its surface, but all three are designed with the aim of removing all particles from the engine bound air. Each technology is different, which gives rise to varying levels of efficacy. The current work uses low order analytical and numerical models to explore these differences and introduces a metric for quantifying the quality of air-particle separation performance. The vortex tube separators exhibit a high efficiency and low pressure drop, but require auxiliary power to operate and experience considerable drag at high forward speeds. Inertial particle separators do not achieve the high separation efficiencies of the vortex tubes or barrier filters, but have a large mass flow to frontal area ratio, hence low drag. Inlet barrier filters are highly efficient at removing particles and improve in this over time due to the accumulation of particles, but at the expense of a temporally increasing pressure drop. The new metric is a quality factor that can be used to directly compare separation technologies for helicopter. Its application is demonstrated by the inlet barrier filter which, when clean, is the best performing device, but over time deteriorates in quality due to the accumulation of particles.

1. INTRODUCTION

The demands of modern day rotorcraft include operation in harsh environments in which dust, sand and other foreign objects may be ingested by the helicopter engine, in particular during a *brownout* landing. In such an environment the engine performance and lifetime are rapidly diminished. Hard, high-inertia particles erode and even plastically deform compressor blades to the extent that chord length is reduced and the flow path is adversely affected. Engine controls compensate by driving the turbine faster, which increases the Mean Gas Temperature (MGT) and accelerates hot-section deterioration, leading to a shortfall in available power. During Operations Desert Storm and Desert Shield in the early nineties, unprotected GE T64 engines were lasting around just 120 hours between removals, nearly depleting the US Navy/Marine Corps inventory of CH-53 engines^[1]. After several decades of operation in such environments, it could now be opined as negligent to omit the use of some variant of engine protection. Fortunately, the demand has been met by the development of a number of key technologies that can be either retro-fitted to the rotorcraft or installed with the engine. These devices are commonly referred to as Engine Air Particle Separation (EAPS) systems.

While performing a vital duty to the engine, the use of EAPS is not without compromise. In addition to system weight and cost, each technology incurs a performance penalty in the form of total pressure loss, added drag, total pressure distortion and in some cases an increase in MGT due to a reduction in mass flow. This may lead to increased specific fuel consumption (SFC), a reduction in hot-end component lifetime when compared against the *clean* or *uninstalled* engine, and a reduction of the engine surge margin. Relating to the engine-rotorcraft system, such effects can be added to the list of sources of

engine installation loss, joining other unwanted problems such as exhaust gas re-ingestion (see Prouty^[2]).

The current work has its origins in a wider aim: to quantify hence predict sources of installed engine performance loss. This paper cross-examines the costs and benefits of each particle separating technology and assesses their operational performance.

2. BACKGROUND

The EAPS systems available generally fall into one of three categories, depending on the particle removal method:

1. Vortex Tube Separators (VTS)
2. Integrated Particle Separators (IPS)
3. Inlet Barrier Filters (IBF).

See Filippone & Bojdo for a review^[3]. The first two utilise *inertial separation*, whereby the particulate-laden fluid streamline is imparted with a change in direction that the particles cannot negotiate due to their inertia. The third type *arrests* the motion of the particle by trapping it within a bed of fibres that is otherwise permeable to the air. The three types are illustrated in Fig.1. The key design goals of an EAPS system are:

1. High separation efficiency (particle removal rate)
2. Low total pressure loss
3. Low total pressure distortion
4. Low weight
5. Low drag
6. Low cost (including maintenance)

These *degrees of freedom* promote competitiveness between the three types of separation device. For example, an IPS has a small frontal area and therefore low drag, but requires bleed air or a pump to operate,

whereas an IBF is passive, requiring no power to function but suffering a higher drag penalty due to particle

accumulation. A summary of the main advantages and disadvantages of each system is given in Table 1.

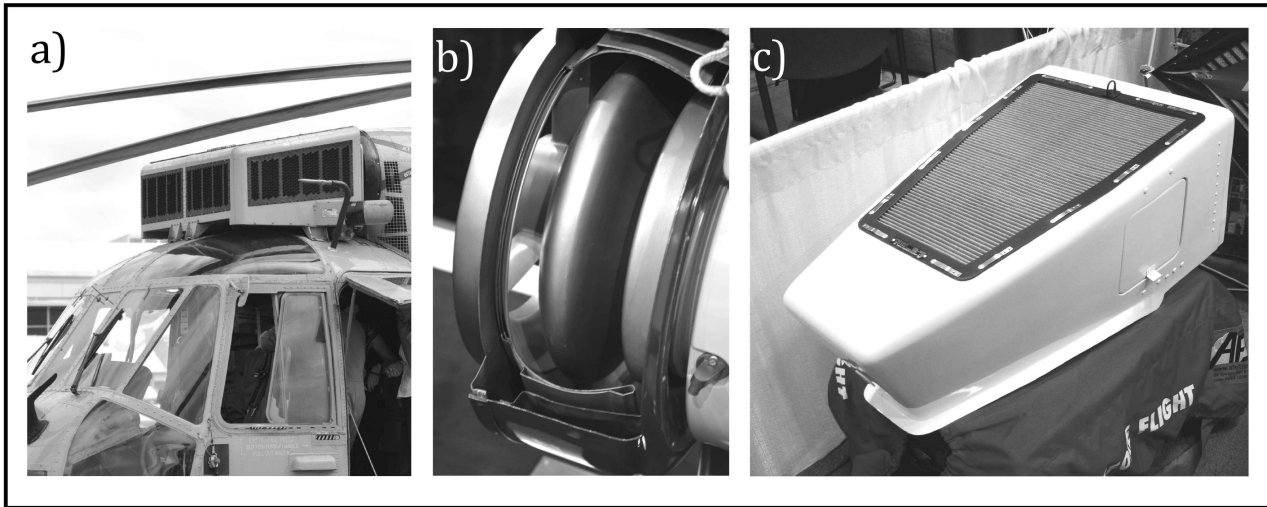


Figure 1: Photographs of the three main EAPS systems; a) Vortex Tubes Separator (elsewhere referred to simply as EAPS); b) Integrated Particle Separator; c) Inlet Barrier Filter.

EAPS Device	Advantages	Disadvantages
Vortex Tube Separators (VTS)	<ul style="list-style-type: none"> • Low pressure loss • High separation efficiency • Bypass door available if needed 	<ul style="list-style-type: none"> • Large frontal area to achieve req. mass flow • Icing issues • Susceptible to FOD • Scavenge pump required • Inlet mass flow extracted to scavenge particles (approx. 5-10%) • Integration difficulties
Integrated Particle Separators (IPS)	<ul style="list-style-type: none"> • High airflow per unit area hence low drag • Easily integrated to engine inlet face • Low total pressure distortion • Ease of optimisation 	<ul style="list-style-type: none"> • Relatively low separation efficiency • Inlet mass flow extracted to scavenge particles (approx. 15-20%) • No bypass capability • Scavenge pump required
Inlet Barrier Filters (IBF)	<ul style="list-style-type: none"> • Very high separation efficiency which increases with use • Reduction of total pressure distribution • No scavenge mass flow • No bleed flow required thus lower MGT over engine lifetime 	<ul style="list-style-type: none"> • Temporally increasing pressure drop due to particle accumulation • Maintenance heavy, thus more time-on-ground (for cleaning/dusting off) • Large surface area required to minimise pressure drop • Integration difficulties

Table 1: Summary of the main advantages and disadvantages of the three EAPS systems.

The three EAPS devices utilise different mechanisms of particle capture, both of which involve a compromise. The VTS and IPS rely on particle inertia and centrifugal force to divert particles into a scavenge conduit, the former by way of a helical vane, the latter by way of a deflector hump. In these systems, high efficiency is achieved at the expense of auxiliary power and a cut of the inlet mass flow to scavenge away the unwanted particles to the atmosphere. The IBF, conversely, passively captures particles in a mat of woven or randomly assorted fibres (approximately 15 micrometer diameter), with the aid of an

oil-based tacking agent. While no auxiliary power is required, the captured particles contribute to a loss in pressure to friction and demand that the filter be regularly cleaned.

All EAPS devices are expected to perform differently depending on the rotorcraft and the operating conditions. In all cases, as will be demonstrated, the separation ability of a device is dependent on the particle size, the power required is dependent on the inflow conditions, and the transient performance (if variable) is dependent on the

dust concentration. The particle size will not be monotonic; in the reality of desert operations a wide range of particles can be expected to reach the engine face. However, an EAPS design will probably be optimised for a single *target* particle diameter that may represent an anticipated particle size distribution. Deviation from this target may lead to a shortfall in efficiency, hence it is important to understand the environment of operation. Similarly, thanks to the dependence of particle inertia on velocity, density and fluid viscosity, a change in inlet conditions such as a reduction in engine mass flow or forward speed can affect the performance of an installed EAPS system. Additionally, a study by Leishman et al.^[4] revealed that brownout cloud severity is very much a function of rotor disk parameters such as tip speed, blade chord length, and disk loading, that affect or effect the mechanisms responsible for sediment uplift. If a particular helicopter is susceptible to intense dust clouds, it may be wise to choose a technology whose performance does not degrade over time. The present work considers these, and aims to establish a method to compare each technology and enhance the decision-making process for selecting the most suitable device.

2.1. Vortex Tube Separator Theory

There is no central core of literature based around EAPS; much of the analysis on similar systems has been performed within the field of *filtration & separation* or intake aerodynamics. As a starting point for low order models and qualitative descriptions of particle separation processes, the book *Fundamentals of Particle Technology* by Holdich^[5] is a valuable resource. The technology behind vortex tube separators is developed from cyclone separators used, for example, in bagless household vacuum cleaners. In this embodiment, particulate-laden air enters a cylindrical chamber tangentially causing fluid rotation within the chamber and a subsequent radial imbalance in particulate concentration which can be bifurcated. However, such devices rely on large mass flow rates and thus power consumption, which is at a premium for helicopters. On a smaller scale, an embodiment known as an *inline* vortex separator can be utilised, wherein the flow enters a tube axially and maintains this axial direction whilst a swirl component is applied via static helical vanes. This is depicted in Fig. 2, which is taken from a patent of a vortex tube separator for helicopter applications. This depiction is typical of the tubes used widely today. A plurality of such tubes is arranged on one or more panels which comprise a box that sits in front of the engine air intakes. There must be a sufficient number of tubes to supply the engine with mass flow. Not shown in Fig. 2 is the scavenge chamber into which the particles are drawn, and the extension of the collector tube through the depth of this scavenge chamber to a sealed cavity that becomes the engine intake duct.

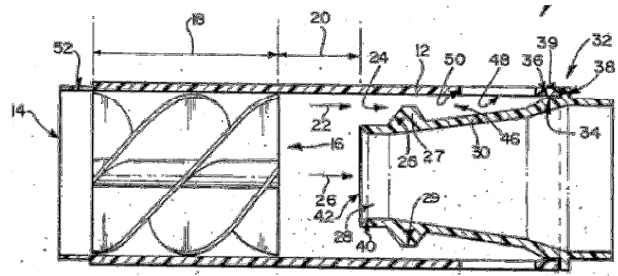


Figure 2: Example of a vortex tube separator, an example of an inline cyclonic separator^[6].

The flow inside a vortex tube separator is complex and not fully understood. Empirical and semi-empirical models have been developed, but their usefulness is often limited to the geometry. Additionally, there are many factors that affect the device performance. The key geometrical design parameters are the helix pitch, number of blades, outer tube diameter, inner tube (known as the *collector*) diameter, and axial distance between the helix and the collector. Furthermore, the behaviour changes according to the axial velocity, which is a function of mass flow rate. Owing to this large array, much of the literature contains case-specific computational fluid dynamics (CFD) studies verified with experimental results. Klujzso et al.^[7] conducted a parametric study on an inline cyclone separator, concluding: that increasing the blade pitch angle improved separation at the expense of pressure drop; that there is a limiting axial velocity for a given tube beyond which separation efficiency does not improve; that gradual turning of the flow reduces pressure loss; and that the implementation of a back cone aft of the helix can enhance performance by displacing a separated flow region in which inadvertent mixing would otherwise draw unwanted particles into the core. However unlike the VTS in Fig. 2, the scavenge chamber in Klujzso's work was not fluidised. A similar study by Hobbs^[8] on a much larger scale demonstrated the case-specific nature of CFD of vortex tubes.

In the present work, the vortex tubes are required to supply a sufficient mass flow of clean air to a helicopter engine. Due to the wide range of intake geometries and engine sizes, it is probable that no single design is optimum for all rotorcraft. Therefore a more general analytical model is required that can be used for an initial, low order prediction of VTS performance and can be applied to numerous embodiments of the vortex tube separator. Such a mathematical model was derived by Ramachandran et al.^[9] to predict the separation efficiency and pressure drop of an inline cyclone separator. The authors verified the model with experimental data and illustrated a good prediction, despite using simplifying assumptions. The validation was conducted with aerosol particles that migrated radially under centrifugal force, and adhered to the tube walls where they could be counted. This differs from the embodiment shown in Fig. 2, in which particles are captured once they breach a radial position equal to the diameter of the inner tube (collector).

2.1.1. Pressure Drop Prediction

Assume the vortex tube resembles the embodiment shown in Fig. 2, with the exception of having parallel,

instead of divergent, collector walls. The axial velocity of the particles and the air is assumed to be equal on entering the tube. The mass of the particles entering is dependent on the mass concentration of the particulate, c_p , but is considered to be sufficiently small to allow the axial velocity of the air-particle mix V_g , to be calculated by applying conservation of mass for the gas alone^[3]:

$$(1) \quad V_g = \frac{\dot{m}_g (1 + c_p)}{\rho_g A_t - \rho_g A_p + \rho_p A_p} \approx \frac{\dot{m}_g}{\rho_g A_t}$$

The particles are thrown to the periphery of the tube by a 4-bladed (cross-shaped profile) helical vane, which has a pitch P_t defined as the axial distance travelled by the gas in one revolution of the helix. The tangential velocity of the gas at a distance r from the axis of the cylinder is

$$(2) \quad V_\theta = 2\pi r \frac{V_g}{P_t}$$

It is assumed that there is no radial component of velocity, that the axial component is invariant along the tube, and that the tangential component varies with radial position. The net velocity of the gas is the vector sum of these two components

$$(3) \quad V = \sqrt{V_g^2 + V_\theta^2} = V_g \sqrt{1 + \left(\frac{2\pi r}{P_t}\right)^2}$$

V varies from a minimum at $r = 0$ to a maximum at $r = R_t$, the tube radius. The average velocity, V_{avg} through the helix section of the tube can be calculated as an area-weighted average of V , which simplifies to

$$(4) \quad V_{avg} = V_g \frac{4\pi}{3R_t^2 P_t} \left[\left(\frac{P_t^2}{4\pi^2} + R_t^2 \right)^{3/2} - \left(\frac{P_t}{4\pi} \right)^{3/2} \right]$$

The pressure drop through the tube is a sum of the loss due to friction and the dynamic pressure required to fluidise the tangential velocity component in the helix. The loss due to friction is calculated for each section of the separator: the helix, the separating region (between the helix and the collector), the collector, and the scavenge conduit (the annulus between the collector and tube walls). The loss is calculated from the Darcy-Weisbach relationship for flow through a cylinder:

$$(5) \quad \Delta P_f = \rho_g \frac{fLV^2}{2D_H}$$

Where f is the friction factor, L is the section length, V is the average gas velocity through the section, and D_H is the section hydraulic diameter. The friction factor is given by^[10]

$$(6) \quad \sqrt{\frac{1}{f}} = -1.8 \log_{10} \left[\frac{6.9}{Re_g} + \left(\frac{\varepsilon/D}{3.7} \right)^{1.11} \right]$$

Where Re_g is the Reynolds number of the cylinder flow, D is the cylinder diameter and ε is the surface roughness. The vortex tube is assumed to be smooth at this point, therefore $\varepsilon/D=0$. The Reynolds number is given by

$$(7) \quad Re_g = \frac{\rho_g V D_H}{\mu}$$

Where ρ_g is the density of the gas. The hydraulic diameter for each section is different. For the helix, it is calculated from

$$(8) \quad D_{H,h} = \frac{4\pi R_t}{(2\pi + 2N_h)}$$

Where N_h is the number of helical vanes. For the separating region and collector it is equivalent to their respective diameters ($D_{H,v}=R_t$ and $D_{H,c}=R_c$); and for the scavenge conduit it is given by

$$(9) \quad D_{H,s} = D_t - D_c$$

The pressure drop due to the required dynamic pressure through the helix is given by

$$(10) \quad \Delta q_h = \rho_g \left(\frac{V_{avg}^2 - V_g^2}{2} \right)$$

If the vortex tube is facing forwards and the rotorcraft is moving forwards, there is an additional term to include to account for ram pressure, given by

$$(11) \quad \Delta q_\infty = \rho_g \left(\frac{V_\infty^2}{2} \right)$$

In the interests of VTS performance prediction, the total tube pressure drop can be segregated into two parts: the *core* pressure drop of the air flow continuing to the engine, and the *scavenge* pressure drop of the proportion of flow to be ejected with the separated particles. It assumed that the pressure distribution at the collector face is uniform, hence the pressure loss at the entry to both the collector and the scavenge is a summation of the helix pressure loss and the separating region pressure loss; the remaining pressure loss for the collector and scavenge are calculated from Eq. (5) using the respective hydraulic diameters. The pressure drop of the tube core is thus

$$(11) \quad \Delta P_c = \Delta P_{f,h} + \Delta q_h + \Delta P_{f,v} + \Delta P_{f,c} - \Delta q_\infty$$

While the pressure drop of the scavenged proportion of flow is

$$(12) \quad \Delta P_s = \Delta P_{f,h} + \Delta q_h + \Delta P_{f,v} + \Delta P_{f,s} - \Delta q_\infty$$

2.1.2. Separation Efficiency Prediction

Entering the helix, the particles will experience three forces: a centrifugal force F_c caused by its helicoidal motion; a buoyancy force B caused by the displacement of gas; and an aerodynamic force D_p , which is equal to the Stokes' resistance. For a particle of radial position r , they are given by the following:

$$(13) \quad F_c = \frac{1}{6} \pi \rho_p d_p^3 \frac{V_\theta^2}{r}$$

$$(14) \quad B = -\frac{1}{6} \pi \rho_g d_p^3 \frac{V_\theta^2}{r}$$

$$(15) \quad D_p = 3\pi d_p \mu U_r$$

Where μ is the viscosity of the gas. Assuming the process has reached steady state, the balance of forces is:

$$(16) \quad F_c + B + D_p = 0$$

Which can be solved for the particle's radial velocity:

$$(17) \quad V_{pr} = \frac{(\rho_p - \rho)}{18\mu} d_p^2 \frac{V_\theta^2}{r}$$

Substituting Eq. (2) into Eq. (17), at a radial distance corresponding to the collector radius i.e. $r=R_c$, yields

$$(18) \quad V_{pr,r=R} = \frac{(\rho_p - \rho)}{18\mu} d_p^2 \frac{R_c V_g^2}{P^2}$$

Consider the cylinder depicted in Fig. 2. A mass balance on an infinitesimal slice of length dL of the cylinder gives:

$$(19) \quad Q_g c_p = Q_g (c_p - dc_p) - V_{pr,r=R} (2\pi R_c) c_p dL$$

Where c_p is the concentration of particles entering the slice, $(c_p - dc_p)$ is the concentration of particles leaving the slice, and $V_{pr,r=R} c_p dL$ is the rate of particle removal into the scavenge conduit. Substituting Eq. (18) into Eq. (19), rearranging, and integrating over the length of the separating region L_v , yields

$$(20) \quad \frac{c_{p,l=L_h+L_v}}{c_{p,l=L_h}} = \exp\left(-Q_g \frac{8\pi}{18\mu} d_p^2 \frac{L_v}{R_c^2 P^2}\right)$$

Since the term on the left hand side represents the concentration of particles remaining at the collector entrance, the separation (or *grade*) efficiency can be expressed by:

$$(21) \quad \eta = 1 - \exp\left(-Q_g \frac{8\pi}{18\mu} d_p^2 \frac{L_v}{R_c^2 P^2}\right)$$

The above equation, adapted for the present work from Ramachandran et al.^[9], assumes plug flow of gas through the tube, uniform concentration and complete lateral mixing due to turbulence in each transverse cross-section. It also neglects the situation of particles bouncing off the helical vane or becoming re-entrained in the core flow after deflection from the tube walls, an event that is likely and may hinder or aid separation. These are reasonable assumptions as a first-order approximation.

The cut diameter, d_{50} , is a length commonly used in the design of cyclone separators. For a particular tube and design mass flow, it corresponds to the diameter of particles collected with 50% efficiency. Based on Eq. (21), the cut diameter is

$$(22) \quad d_{50} = \sqrt{\frac{18\mu(\ln 2) R_c^2 P^2}{8\pi \rho_p Q_g L_v}}$$

Which allows the separation efficiency can be expressed in terms of the cut size:

$$(23) \quad \eta = 1 - \exp\left[-\ln 2 \left(\frac{d_p}{d_{50}}\right)^2\right]$$

Hence for a given vortex tube, the separation efficiency can be found for a range of particle sizes.

2.1.3. Power Required

The use of an EAPS system gives rise to up to three additional sources of power loss, which are ultimately catered for by the engine. As part of the assessment it would be useful to compare the total power required to service each device. In the case of vortex tubes, power is required to:

1. Fluidise the scavenge flow for particle ejection.
2. Maintain core mass flow to the engine in the presence of pressure loss to friction across the device.
3. Overcome the additional drag created by the device.

The work done per unit time can be expressed in a number of ways. For the first, the power required is calculated by considering the scavenge mass flow rate and including, this time, the mass of the particles:

$$(24) \quad \dot{m}_s = \dot{m}_{g,s} + \dot{m}_{p,s} = \dot{m}_g (S + \eta c_p)$$

Where S represents the fraction of mass flow required for scavenging particles. Then the scavenge power required is simply

$$(25) \quad W_{s,VTS} = \dot{m}_s \Delta P_s$$

It is likely that this formula under predicts the required power, as there are other sources of pressure loss that are not catered for by Eq. (12). For example, the arrangement of the collector tubes within the scavenge chamber

(analogous to boiler tank tube bundles) is unknown, but it is supposed that considerable power is required for them to be overcome by the scavenge flow.

The power required to maintain core mass flow adopts the same method:

$$(26) \quad W_{c,VTS} = \dot{m}_g (1 - S) \Delta P_c$$

The drag is calculated by considering the total surface area occupied by the tubes and the supporting plan form area. Assuming that all vortex tubes collectively are designed to supply a design point mass flow \dot{m}_E to the engine via each one of their collectors, the number of tubes required is

$$(27) \quad N_t = \frac{\dot{m}_E}{\dot{m}_c} = \rho_g V_g \pi R_c^2$$

If it is assumed that 25% of a VTS panel is required to support the tubes' arrangement, the total drag acting on the panel is

$$(28) \quad D_{VTS} = \frac{1}{2} \rho_g N_t A_t \left(V_\infty^2 - V_g^2 + \frac{1}{3} V_\infty^2 \right)$$

The power required to overcome the drag force is

$$(29) \quad W_{D,VTS} = D_{VTS} V_\infty$$

Summing Eq. 25, 26 and 29 yields the total power required for the VTS system:

$$(30) \quad W_{VTS} = W_{s,VTS} + W_{c,VTS} + W_{D,VTS}$$

2.2. Inlet Barrier Filter Theory

The Inlet Barrier Filter has received little interest in the academic literature, despite its widespread application to rotorcraft worldwide. The early nineties saw a rise in the use of EAPS systems and in particular the vortex tubes, and since then filtration media have become more sophisticated and the technology more developed. Filtration by porous matrices has remained at the forefront of the particle separation field finding wide appeal, from pollution control to industrial dust collection. (See Purchas & Sutherland^[11] for more details). The early- and present-day IBF use woven cotton filters impregnated with an oil tacking agents, but the latest designs feature a new dry synthetic material composed of ultrafine nanofibres arranged randomly in a fibrous bed. While it is the precisely developed fibres of the filter medium which ultimately arrest the motion of an influent particle, the IBF is heavily reliant on *pleating* to achieve a good performance. Folding the filter medium in this way increases the filtration area, which helps to capture more particles and reduces the pressure drop across the medium by decreasing the superficial velocity. While the literature on filter media is vast owing to its lengthy history (dating back to the days of Darcy), studies on pleated filters are less explored. A depiction of a pleated filter is given in Fig. 3.

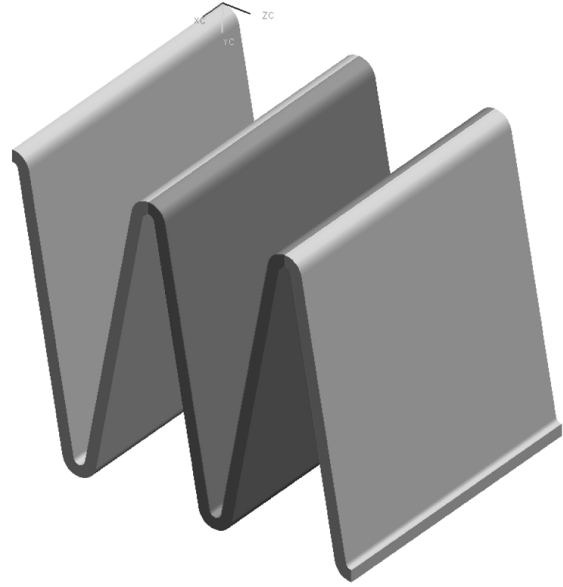


Figure 3: An example of an IBF filter pleat.

The authors^[12-16] that have investigated, by CFD or experimentation, the technique of filter pleating focus on the occurrence of an optimum pleat density (also called pleat pitch, pleat width or pleat count) which arises due to the emergence of a secondary pressure loss within the pleat channels. The optimum design is dependent on several factors, including the filter medium permeability, the degree of clogging, the throughput volume flow rate, the flow properties, and the pleat dimensions. Rebaï et al.^{[17],[18]} developed a semi-analytical model to predict pleated filter performance without the use of CFD. Their model shows good correlation with CFD, and fits a small number of experimental data points. However, their model is limited to low Reynolds number flows and does not account for turbulence.

Recent work by this author aims to apply the practices of the abovementioned to gain a greater understanding of the transient nature of IBF filters. Some recent results are presented within this paper. Due to the wide range of factors that influence the pressure drop across a pleated filter, CFD was used. For a detailed description of the simulation description please see Bojdo & Filippone^[19]. The CFD results are used in the present work to provide pressure drop data across a pleated filter subjected to flow typically encountered by IBF.

2.2.1. Separation Efficiency Prediction

Particle capture by filter fibres is not easy to predict. Aside from the highly unorganised arrangement of fibres within the mat, the main difficulty arises from the variation of the different capture mechanisms with Stokes number. Such theories of fibre-particle interaction are outlined in depth in the books of Davies^[20] and Brown^[21]. The three capture mechanisms are:

- i. *Diffusion*, by which particles are intercepted by fibres as they wander in random Brownian motion, crossing fluid streamlines.
- ii. *Direct Interception*, by which particles follow fluid streamlines around a fibre, but are intercepted by virtue of their bulk.

- iii. *Inertial Impaction*, by which particles possessing too much inertia cannot negotiate the flow path around the fibre and leave the streamline to deposit on the fibre surface.

These are depicted in Fig. 4.

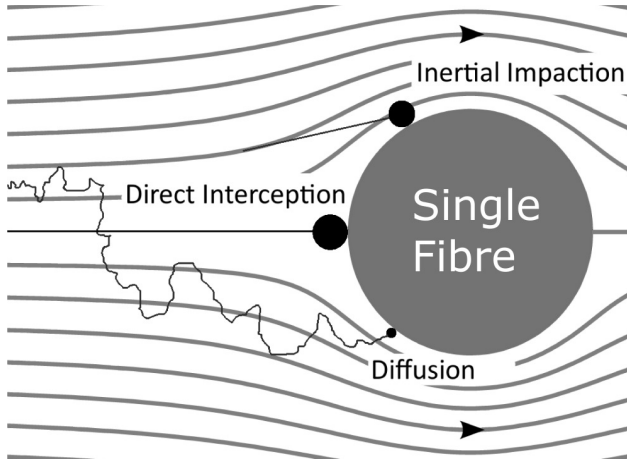


Figure 4: The three single fibre capture mechanisms.

Collectively these mechanisms yield a *single fibre efficiency* which can be combined with the depth and porosity of the whole filter to determine the overall separation efficiency. The single fibre efficiency is a non-linear function of the Stokes Number, which is defined as:

$$(31) \quad St = \frac{d_p^2 \rho_g V_p}{18\mu d_f}$$

Where d_f is the fibre diameter and V_p is the particle velocity, assumed to be equal to the local gas velocity. At low Stokes number, below 0.025, the particle's motion is interfered with by bombardment of gas molecules, as in Brownian diffusion. As the diameter increases, so does the Stokes' drag and the particle begins to follow fluid streamlines. If the particle passes close enough to touch the fibre it may be directly intercepted. Beyond a Stokes number of 0.2 the particle's inertia causes it to cross streamlines. It increasingly fails to negotiate the disturbance to flow caused by the presence of a fibre, and is captured. As particle Reynolds number increase further, the phenomenon of particle bounce may begin to occur, whereby the adhesive forces present at the particle-fibre interface are no longer strong enough and the particle evades capture. At this point along the Stokes number scale there is a temporary dip in collection efficiency. As the diameter increases further, however, there is a rapid rise in capture efficiency as the fibrous mat begins to act like a sieve. These numerous processes make the prediction of particle fate rather difficult.

Fortunately there are formulae available that have been fitted to experimental data and are suitable for application to IBF. One such formula for the inertial impaction efficiency is given in Brown^[22] as:

(32)

$$E_I = \frac{St^3 e^3}{St^3 e^3 + 0.77 \left(1 + \frac{K_3}{Re^{1/2}} + \frac{K_4}{Re} \right) St^2 e^2 + 0.58}$$

Where $e(c)$ is a function of the packing fraction, given by

$$(33) \quad e(c) = 1 + K_1 c + K_2 c^2$$

In Eqs. (32) and (33), the parameters K_1 - K_4 were fitted by least squares to experimental data on real and model filters. These filters had a similar *packing fraction* (opposite to porosity) to the filters used for IBF. In general, the inertial impaction mechanism covers a relatively wide range of Stokes numbers. In this first-order analysis it is satisfactory to exclude the diffusion and direct interception mechanisms and neglect any particle bounce (as with the VTS method).

Once the single fibre efficiency is known for a given Stokes number, the log-penetration rule can be used to determine the overall efficiency of the medium. This is given in Brown^[22] as:

$$(34) \quad \eta_{IBF} = 1 - \exp\left(-\frac{4a_F \Delta z E_I}{\pi(1-a_F)d_f}\right)$$

Substituting Eq. (33) into (32), and (32) into (34) yields an expression for the overall fabric efficiency as a function of particle diameter and influent velocity.

2.2.2. Pressure Drop Prediction

The prediction of pressure drop for the IBF system is made using CFD. A parametric study was conducted to ascertain the optimum pleat design for inflow conditions resembling those expected during IBF operation. The pleat pitch, pleat depth, and filter thickness were all varied, along with the internal properties of the filter such as porosity, permeability (inherent resistance) and fibre diameter. The simulations were performed in two dimensions using the Reynolds Stress Model to solve the Reynolds-Averaged Navier-Stokes (RANS) equations. A second order upwind scheme was used to discretise the pressure and momentum equations, and the PISO scheme was used to solve the pressure-velocity coupling. Independence checks were performed on the grid, which was made up of 210 to 639 thousand mainly triangular cells. A quad pave scheme was adopted in areas of low stress-strain to reduce computation time.

An area of the domain resembling a pleat cross-section was designated as a *porous zone*, in which all cells are prescribed with an additional momentum source term (a sink term) to simulate the friction losses caused by flow through a filter medium. The properties of this source term are user-defined, and can be chosen to reflect a typical filter material used for IBF. One of the aims of the parametric study was to investigate the effect of filter clogging on the pressure drop for different particulate properties. To achieve this, the resistance of the porous

zone was increased step-by-step until the virtual mass accumulated had reached the holding capacity of the medium - an intrinsic property of the filter. At this point, additional areas of the domain were 'activated' as porous zones to resemble the accumulation of particles on the filter surface – a process that generally leads to a larger temporal increase in pressure loss. These surface layers are known as *cake*. To calculate the filter medium viscous and inertial resistance terms, the well-known *Ergun equation* was used^[23]; for the cake resistance terms, a model developed by Endo et al.^[24], which accounts for the effects of polydispersity, was used.

2.2.3. Power Required

As with the vortex tubes, the total power required is a summation of each loss source. The only difference is that the IBF system is passive: it does not require any auxiliary pump to scavenge away the particles. The pressure drop is provided by the CFD data; the drag is given by the following:

$$(35) \quad D_{IBF} = \begin{cases} \frac{1}{2} \rho_g A_F (V_\infty^2 - V_F^2) & \text{for } V_\infty \geq V_F \\ D_{IBF} = 0 & \text{else} \end{cases}$$

Substituting Eq. (35) into (29) for D_{VTS} and summing the power contributions for IBF gives

$$(36) \quad W_{IBF} = W_{F,VTS} + W_{D,VTS}$$

2.3. Integrated Particle Separator Theory

The final type of EAPS system to be investigated is the IPS. In contrast to the other particle separators, the literature is rich with studies on this device. This is perhaps due to the relatively simple design (see Fig. 5) that renders this device more amenable to CFD modelling. In fact, derivation of an analytical model for the separation efficiency is made more cumbersome by the fact that due to the engine inlet proximity, the inlet velocity is very high: particles enter with a great deal of momentum, which elevates the importance of predicting collision and rebound characteristics. The embodiment shown in Fig. 5 is an axial IPS (radial types also exist). Flow enters and is immediately forced radially outwards by a *hump*, before being bifurcated by a *splitter*, whose role it is to segregate the clean and dirty air. The inertial separation principle again applies, with the radially extreme particles being scavenged to the atmosphere with 15-20% of the inlet mass flow. The cleaner air is drawn radially inwards after the hump, and continues to the engine.

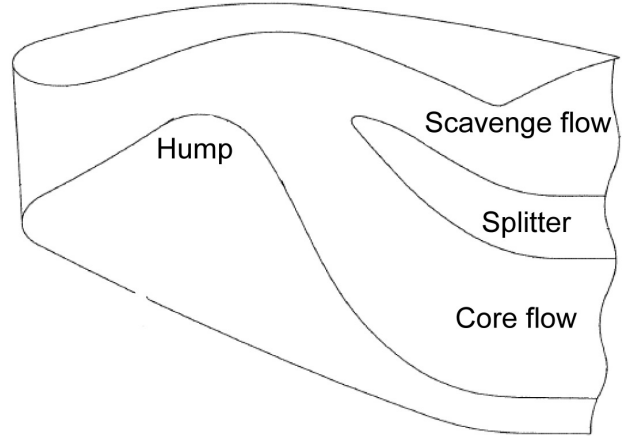


Figure 5: Diagrammatic drawing of a simple integrated particle separator.

The majority of the literature pertains to RANS solutions of fully turbulent flow through case-specific embodiments of the axial IPS shown in Fig. 5. Particles are tracked in the Lagrangian frame using a combination of deterministic and stochastic bounce models, which are integrated within the RANS solution until impact with a wall, upon which new initial conditions are produced^{[25],[26]}. The most recent work is that of Taslim et al.^{[27],[28]}, in which they diminished previously erroneous results by applying elastic restitution coefficients to the impact boundary conditions. They also investigated parameters that could affect separation efficiency such as inlet angle and sand density, and found that particles of diameter less than 20 μm could not easily be separated, since they followed gas streamlines to the engine, but also found that such particles were also more sensitive to changes in particle shape factor.

To conduct a full numerical simulation of an IPS system would be both time-consuming and rather futile given the lack of experimental data for validation or case-specific geometrical details. However, developing an analytical solution is also tricky given the complex nature of the particle trajectories. To facilitate comparison between the three technologies, therefore, the present work adopts the results of Taslim et al. and uses properties of the same engine to predict VTS and IBF performance, as if all devices were to operate with the same powerplant. From their work it is possible to extract data pertaining to the core flow and scavenge flow pressure losses as a function of engine mass flow for four intake geometries. For a single mass flow setting it is also possible to use the calculated separation efficiencies for a range of particle sizes.

2.3.1. Power required

Unlike the IBF, the IPS is not a passive separating system: it requires a scavenge pump or ejector to run. However, the mass flow per unit frontal area is comparatively large which means there is very little additional drag (negligible). The power summation thus reduces to:

$$(37) \quad W_{IPS} = W_{c,IPS} + W_{s,IPS}$$

Where $W_{c,IPS}$ and $W_{s,IPS}$ are calculated as per Eqs. (25) and (26).

2.4. EAPS Quality Factor

The objective of this study is to compare EAPS technologies. Three variables have already been highlighted for analysis: separation efficiency, pressure drop, and required power. A fourth method exists within the field of filtration and separation, which combines both the loss in pressure and separation ability of a given filter in order that different designs for the same purpose can be assessed overall. It is known as a Filter Quality Factor. A neat explanation is given in Brown: since pressure drop is related to the energy expenditure in filtration, the quotient of the logarithm of the penetration ($1-\eta$) and the pressure drop is a measure of the performance achieved against the energy expended. The quality factor is given by:

$$(38) \quad QF = \frac{-\ln(1-\eta)}{\Delta P}$$

Good filters given high efficiency and low pressure drop, thus larger values of QF indicate better performance. This formula has been applied elsewhere in the literature to evaluate filter performance when a large number of parameters need to be compared^[29]. Given that both pressure loss and separation efficiency are functions of inflow conditions and particulate properties, this formula is a useful tool for comparison.

3 RESULTS AND DISCUSSION

The technologies are first dealt with in turn, to illustrate their individual effectiveness in the main assessment criteria. In each case, where applicable, consistent parameter ranges were used. Each device was designed to protect an engine with a design point mass flow of 6.25 kg/s⁻¹; between hover and 30kt forward flight; and from two differing particle size distributions resembling Arizona AC Fine and Arizona AC Coarse test dust.

3.1. Vortex Tube Separator Performance

The design of vortex tubes can be optimised, as has been shown in the literature. However, there are a great number of parameters to consider in this process; to discuss at length the various permutations at this stage, especially when there are no experimental data with which to verify the results, is beyond the scope of the current work. Instead, the tube diameter and design point tube mass flow rate are borrowed from the patent^[6] that bore the graphic in Fig. 2. The dimensions are as follows:

- Outer tube diameter 18 mm
- Tube length 60 mm
- Helix length (= pitch) 20 mm
- Collector mass flow 4.4 gs⁻¹
- Scavenge proportion 8 %

Other dimensions, such as the collector length, had to be estimated. The fluid properties assumed their static sea level values. The particle density was 2700 kgm⁻³ and particles were assumed to be spherical.

3.1.1. Separation Efficiency

To express the separation efficiency in a meaningful way, the grade efficiency as expressed by Eq. (23) can be applied to each particle group of a known particle size distribution (PSD). For example, consider a PSD in which 20% of the range is comprised of 10µm particles. If the vortex tube can separate 10µm diameter particles with 80% efficiency then 16% of the 10µm group will be scavenged. The overall fraction of particles removed, i.e. the total separation efficiency of the PSD, is simply the summation of each particle group's scavenged fraction. Figure 6 shows the effect of engine mass flow on overall separation efficiency of two particle size distributions. The increase in efficiency with mass flow is attributable to the increase in axial velocity hence tangential velocity and particle angular momentum. Despite the shortfall in efficiency between fine and coarse test dusts, the VTS still manages to achieve a substantial efficiency of around 78% at a low mass flow rate of 1 kg/s⁻¹.

3.1.2. Power Required

Figure 7 shows the breakdown of required power to service the VTS. During hover there is around seven times more power required to overcome the core flow pressure drop than scavenge away the particles. This may change if the energy require to overcome resistance in the scavenge chamber is included in the model. The pressure loss power is expected to decrease with forward speed thanks to ram pressure recovery. However in reality not all vortex tubes will not be orientated into the wind, so the saving in power is perhaps generous.

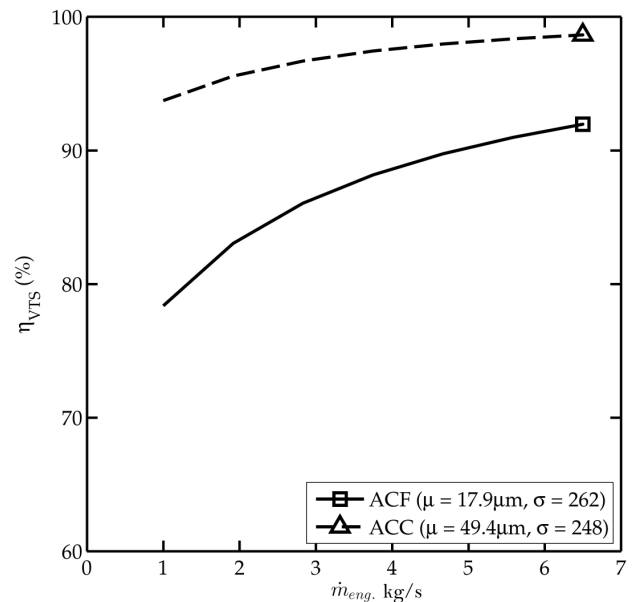


Figure 6: Separation efficiency as a function of engine mass flow rate, for VTS.

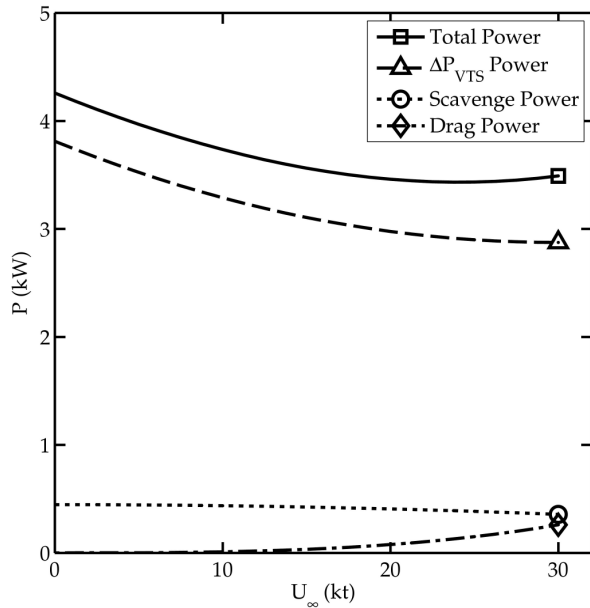


Figure 7: 'Power required' breakdown as a function of forward speed, for VTS.

3.2 Inlet Barrier Filter Performance

The choice of geometry for the filter pleat was based on data acquired during design optimisation studies. There are two optimum design points. The first is the pleat half-angle (angle between the pleat line of symmetry and fold angle) at which minimum pressure loss occurs when the filter is clean. This is usually around 7 degrees. The second optimum design corresponds to the half-angle that can hold the greatest mass of particulate for a given loss on pressure. Since a higher pleat density increases the filtration surface area, it follows that the optimum angle for maximum *holding capacity* (at $\Delta P_F = 3000\text{Pa}$) is around 1 or 2 degrees. The ideal design therefore is one in which both optimums are satisfied. In the present work, this leads to a pleated filter of dimensions:

- Pleat depth 50 mm
- Pleat half-angle 3 degrees
- Filter thickness 1.5 mm

Other properties, such as the initial filter permeability and fibre diameter are unknown for the IBF and are therefore taken from Rebai et al.^[17], which has its application in the automotive industry.

3.2.1. Separation Efficiency

Applying the same logic as in Section 4.1.1., the separation ability of an inlet barrier filter can be assessed over a range of particle sizes and mass fractions that resemble the two featured particle size distributions. The results are shown in Fig. 8. As with the VTS, there is a decrease in efficiency of both distributions as the mass flow rate decreases. In this case the superficial velocity decreases, which effectively reduces the Stokes number given by Eq. (31) hence diminishes the single fibre efficiency. What these results illustrate is the importance of component design. In the end, the helicopter is most at risk during hover, when it is likely to be exercising

maximum mass flow. This is the design point target for which these systems were designed. However it may be worth sacrificing a greater pressure loss at full mass flow by reducing the design point target mass flow, to ensure that the separation efficiency is maintained when the engine mass flow drops from the maximum.

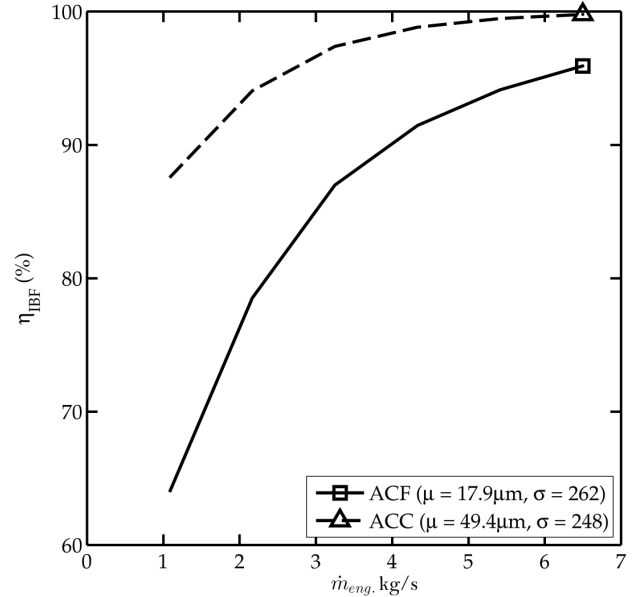


Figure 8: Separation efficiency as a function of engine mass flow rate, for IBF.

3.2.2. Transient Pressure Drop

It was mentioned in the introduction that IBF suffer the undesired side-effect of particle capture: a temporally rising loss in pressure. This arises from the additional drag exerted on the fluid by the continually accumulating particles. Figure 9 illustrates the speed of pressure deterioration for three different particulate concentrations. 5 gm^{-3} represents the upper limit or peak concentration, which probably occurs during the brief hover close to the ground when the rotor disk re-ingests disturbed sediment from the ground. In reality such peaks are unlikely to last the order of minutes; the line corresponding to 1 gs^{-1} may be a more appropriate prediction as an average. In any case, the timescales are not long; and beyond 3000Pa the pressure loss becomes rather troublesome for the pilot. The results support the anecdotal evidence that filters become so heavily soiled after each brownout landing that the modules are removed from their housing and tapped clean.

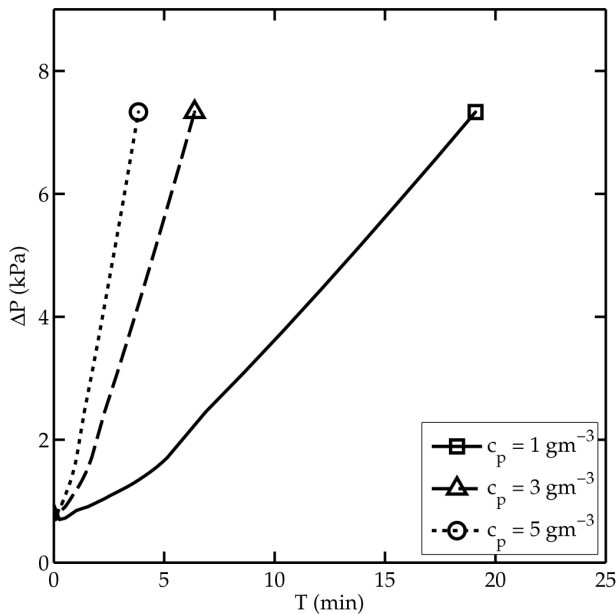


Figure 9: Temporal pressure drop across an IBF pleat due to particle accumulation.

3.2.3. Temporal Separation Efficiency

A benefit of particle accumulation is an improvement in the overall filter separation efficiency. As particles collect within the filter the pores decrease in size, restricting flow and allowing more particles to be captured. This is illustrated in Fig. 10.

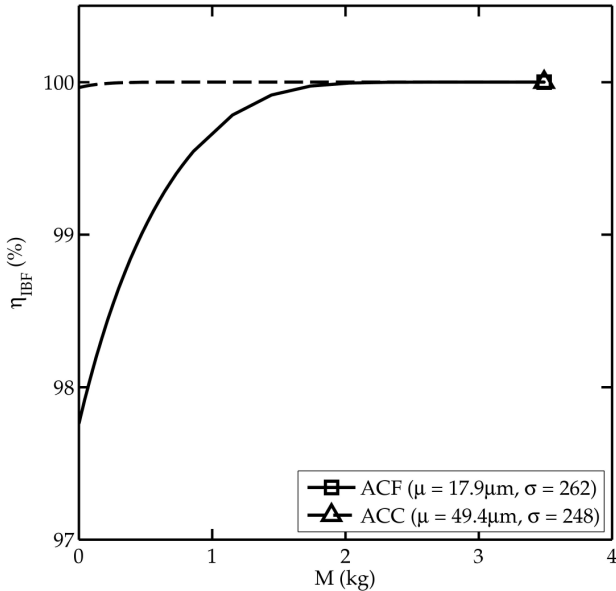


Figure 10: Improvement in particle separation efficiency as a function of collected particulate mass by the IBF.

3.3. Integrated Particle Separator Performance

Since all results for the IPS performance prediction was taken from another author's study, there is limited data to show.

3.3.1. Power Required

A breakdown of the power required to service an integrated particle separator is given in Fig. 11. As occurred with the VTS device, the scavenge power is a fraction of the power required to overcome the losses in the core flow – around 20%. There is a reduction in required power with forward speed, and unlike the VTS and IBF devices there is no rising drag force: the required power will continue to fall.

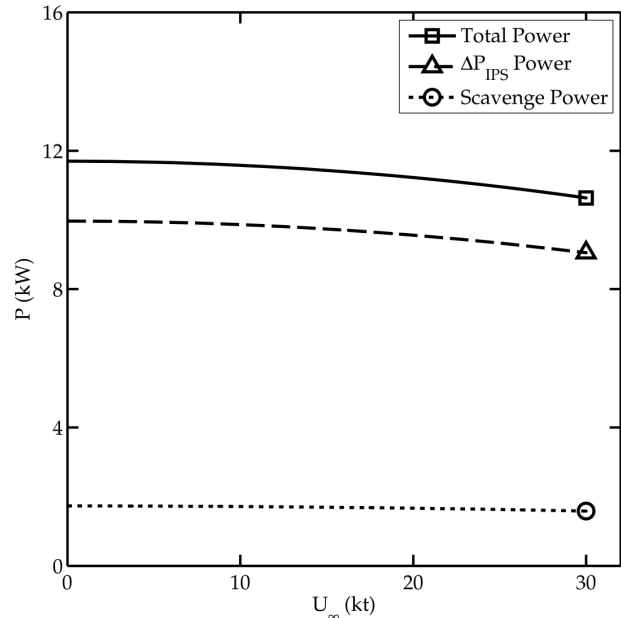


Figure 11: Required power breakdown as a function of forward speed for IPS.

3.4. EAPS Technology Cross-comparison

3.4.1. Separation Efficiency

The cross-comparison begins by examination of separation efficiency. By superimposing the grade efficiency of each device on to the cumulative density function (CDF) of the PSD in question it is possible to make a visual comparison of the technology. Figures 12 and 13 show the EAPS performance when subjected to Arizona AC Fine (ACF) and Arizona AC Coarse (ACC) dusts respectively. In both instances the IBF performs best and the IPS performs worst, although the difference between the IBF and VTS is only slight, when filtering AC Coarse dust. The separation achievement of AC Coarse dust is markedly better than its performance. In fact the figure overall efficiency in filtering AC Coarse dust is around 83 %, which is at least comparable to the other technologies. Subjected to even coarser sand, the IPS may out perform the VTS. With the inclusion of a particle bounce model in the VTS prediction it would be interesting to investigate whether the IPS can surpass its current capabilities.

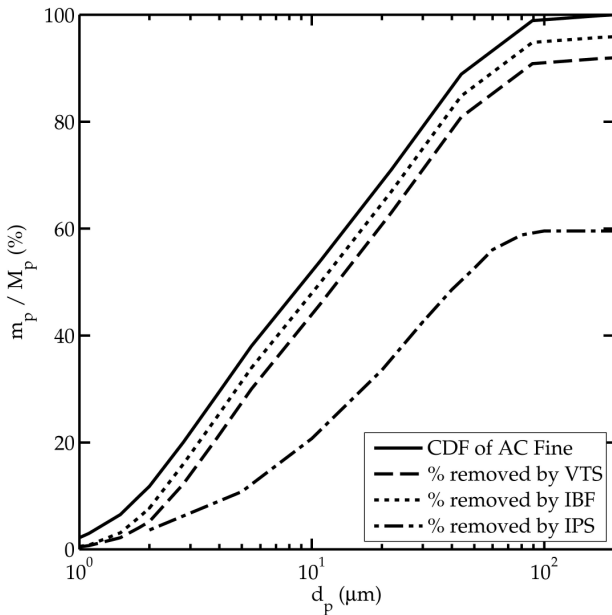


Figure 12: Graded separation efficiency of the three EAPS technologies when filter AC Fine test dust.

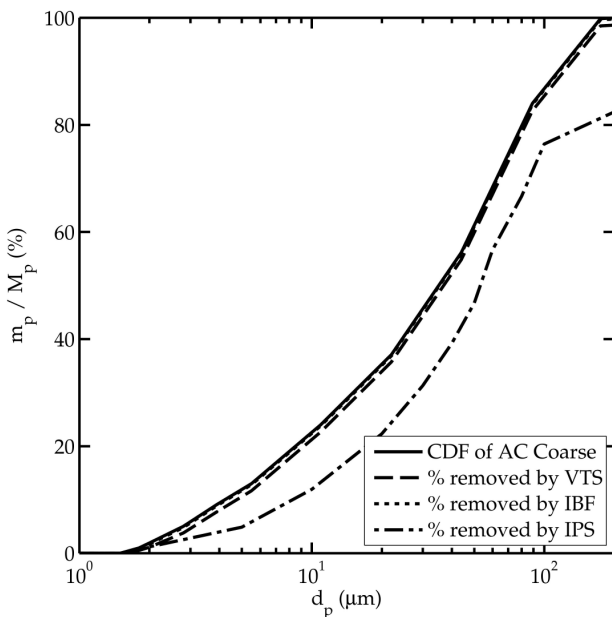


Figure 13: Graded separation efficiency of the three EAPS technologies when filter AC Coarse test dust.

3.4.2. Power Required

The next performance indicator accounts for all aspects of energy loss as a consequence of EAPS installation. By combining the power lost to friction across the device, to servicing any scavenge lines, and to drag, the devices can be compared fairly.

Figure 14 shows the power requirement as a function of engine mass flow rate. Of the three, the IPS device requires the most power, while the IBF only performs best at low mass flow rates. Engines demand high mass flow rates when there is a request for additional power, such as during takeoff and landing, or heavy lift. In these conditions an extra few percent of power can be extremely

important. With an EAPS device fitted, the consequential shortfall in available power is clear from Fig. 14. While the models used to predict these trends are low order, they show that the cost of fitting pre-inlet EAPS devices is not insignificant.

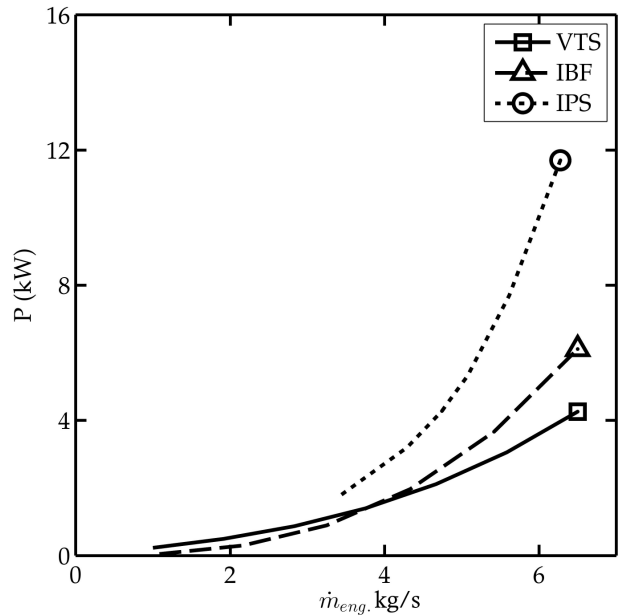


Figure 14: Variation in required power for the three EAPS technologies as a function of engine mass flow rate.

3.4.3. EAPS Quality Factor

The EAPS quality factor was introduced to gather the key filtration assessment parameters together. It is used to directly compare different filters designed to perform the same duty, to ascertain the most suitable configuration for the task. It must be used with caution since, for example, a high QF may appear good, but the value does not give an indication as to whether the quality is derived from a high separation efficiency or a low pressure drop. It should be used in conjunction with known values of pressure drop and efficiency, but can also be useful in ascertaining a quick assessment of separation device quality.

Figure 15 demonstrates the usefulness of this tool. The EAPS Quality Factor is plotted as a function of mass captured specifically by the IBF during hover, with the engine running at the design mass flow rate (although since the mass flow rate is the same for each device the abscissa may also represent the total mass filtered by each device). Interestingly, the IBF begins as the best performing EAPS device, just ahead of the VTS. However, despite the associated increase in collection efficiency, as particles collect the rise in pressure drop leads to a reduction in quality factor. After collecting approximately 5 kg of particulate the IBF becomes the worst performing device. In reality, this situation is unlikely to occur because the IBF will not be permitted to reach such a severe level of clogging. However, the extrapolation really contextualises the degradation of pressure experienced by an IBF. It also highlights the gulf between the different technologies' performances as a result of different pressure drop and separation efficiency.

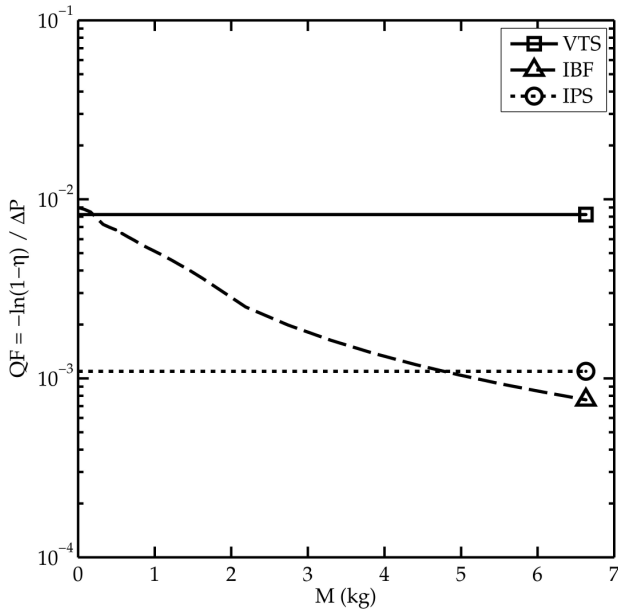


Figure 15: Comparison of EAPS devices by Quality Factor, as a function of captured AC Coarse test dust.

The EAPS quality factor may also be used to compare device performance across the range of mass flow rates. Whilst the EAPS is generally required when the engine mass flow is high (during take-off and landing), the assessment parameter can be used to determine whether one device performs better during forward flight. All systems are designed to remain fixed in position therefore any pressure loss incurred is carried with the rotorcraft. Figure 16 shows the effect of engine mass flow on EAPS quality factor. In all cases there is a decrease in quality factor with an increase in engine mass flow. This implies that the increase in pressure loss with mass flow is not completely 'paid for' by the improvement in separation efficiency. It seems that the VTS and IBF perform better than the IPS, with the VTS performing the best.

4 CONCLUSIONS

Across the spectrum of EAPS devices are dozens of parameters that combine to complicate the assessment of separator system efficacy. In particular, some devices' performance is time dependent, while others' performance relies upon auxiliary power. By aligning some of the many variables and creating a new assessment tool, the present work has made the comparison of EAPS systems more translucent. The main conclusions are:

1. The use of EAPS systems is undeniably beneficial to engine performance in harsh environments, but their use can incur a large penalty to the powerplant system, in the order of kilowatts.
2. Vortex Tube Separators and Inlet Barrier Filters appear to perform better than Inertial Particle Separators both in pressure loss characteristics and separation efficiency. However, no certain claims are being made due to a lack of real scientific data.
3. In all cases of EAPS systems there is an improvement in separation efficiency at the

expense of pressure loss as engine mass flow hence particle velocity increases.

4. Inlet Barrier Filters perform best when they are clean. As particles accumulate a performance benefit is experienced by way of a separation efficiency, but this is more than negated by an increase in pressure loss.
5. The smaller and slower-moving the particle, the more difficult it is to remove from the air. However, EAPS devices can be designed for a target particle size and mass flow rate to ensure optimum performance. Hence knowledge of the rotorcraft and operating environment are very important.

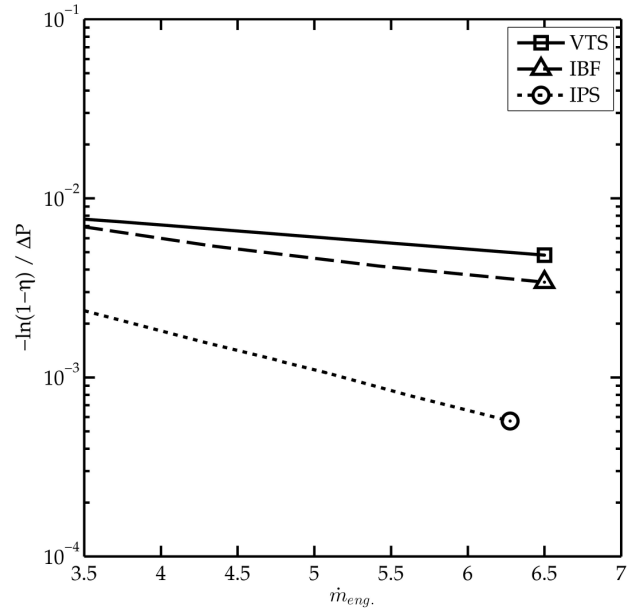


Figure 16: Comparison of EAPS devices by Quality Factor when experiencing a particulate of AC fine test dust, as a function of engine mass flow rate.

REFERENCES

- [1] F. Colucci, "Safety Spotlight: Enduring Power," *Vertifilte*, vol. 53, no. 2, pp. 25–27, Summer-2007.
- [2] R. W. Prouty, *Helicopter performance, stability, and control*. PWS Engineering, 1986.
- [3] A. Filippone and N. Bojdo, "Turboshaft engine air particle separation," *Progress in Aerospace Sciences*, vol. 46, no. 5–6, pp. 224–245, July.
- [4] J. Milluzzo and G. Leishman, "Assessment of Rotorcraft Brownout Severity in Terms of Rotor Design Parameters," *Journal of the American Helicopter Society*, vol. 55, no. 3, pp. 032009–1, 2010.
- [5] R. G. Holdich, *Fundamentals of particle technology*. Midland Information Technology and Publishing, 2002.
- [6] W. J. C. Prinsloo, P. D. Villiers, and M. C. V. Dijken, "Vortex Tube Separating Device," U.S. Patent 498505815, Jan 1991.
- [7] L. A. C. Klujzso, P. K. Songfack, M. Rafaelof, and R. K. Rajamani, "Design of a stationary guide vane swirl air cleaner," *Minerals engineering*, vol. 12, no. 11, pp. 1375–1392, 1999.

- [8] A. Hobbs, "Design and Optimization of a Vortex Particle Separator for a Hot Mix Asphalt Plant."
- [9] O. Ramachandran, P. C. Raynor, and D. Leith, "Collection efficiency and pressure drop for a rotary-flow cyclone," *Filtration and Separation*, vol. 31, no. 6, pp. 631–636, 1994.
- [10] F. M. White, *Fluid Mechanics*, 2nd ed. McGraw-Hill, New York, 1986.
- [11] D. P. Purchas and K. Sutherland, *Handbook of Filter Media*, 2nd ed. Elsevier, 2002.
- [12] C. W. Chen, S. H. Huang, C. M. Chiang, T. C. Hsiao, and C. C. Chen, "Filter quality of pleated filter cartridges," *Annals of Occupational Hygiene*, vol. 52, no. 3, p. 207, 2008.
- [13] A. Subrenat, J. N. Baléo, and P. Le Cloirec, "Analysis of pressure drops in pleated activated carbon cloth filters," *Journal of Environmental Engineering*, vol. 126, no. 6, pp. 562–568, 2000.
- [14] T. Lücke and H. Fissan, "The prediction of filtration performance of high efficiency gas filter elements," *Chemical Engineering Science*, vol. 51, no. 8, pp. 1199–1208, Apr. 1996.
- [15] R. J. Wakeman, N. S. Hanspal, A. N. Waghode, and V. Nassehi, "Analysis of pleat crowding and medium compression in pleated cartridge filters," *Chemical Engineering Research and Design*, vol. 83, no. 10, pp. 1246–1255, 2005.
- [16] N. Bojdo and A. Filippone, "Performance Prediction of Inlet Barrier Filter Systems for Rotorcraft Engines," *Journal of aircraft*, vol. 48, no. 6, pp. 1903–1912.
- [17] M. Rebai, M. Prat, M. Meireles, P. Schmitz, and R. Baclet, "Clogging modeling in pleated filters for gas filtration," *Chemical Engineering Research and Design*, vol. 88, no. 4, pp. 476–486, 2010.
- [18] M. Rebaï, M. Prat, M. Meireles, P. Schmitz, and R. Baclet, "A semi-analytical model for gas flow in pleated filters," *Chemical Engineering Science*, vol. 65, no. 9, pp. 2835–2846, May 2010.
- [19] N. Bojdo and A. Filippone, "Helicopter Engine Inlet Barrier Filter Design," in *37th European Rotorcraft Forum*, MAGA Gallarate (VA), Italy, 2011, pp. 639–648.
- [20] C. N. Davies, *Air Filtration*. Academic Press, 1973.
- [21] R. C. Brown, *Air Filtration: An Integrated Approach to the Theory and Applications of Fibrous Filters*. Pergamon Press, 1993.
- [22] R. C. Brown, *Air Filtration: An Integrated Approach to the Theory and Applications of Fibrous Filters*. Pergamon Press, 1993, pp 86-87.
- [23] J. Bear, *Dynamics of Fluids in Porous Media*, 1st ed. Elsevier, 1972.
- [24] Y. Endo, D.-R. Chen, and D. Y. H. Pui, "Effects of particle polydispersity and shape factor during dust cake loading on air filters," *Powder Technology*, vol. 98, no. 3, pp. 241–249, Aug. 1998.
- [25] A. Hamed, Y. D. Jun, and J. J. Yeuan, "Particle Dynamics Simulations in Inlet Separator with an Experimentally Based Bounce Model," *Journal of Propulsion and Power*, vol. 11, no. 2, pp. 230–235, 1995.
- [26] B. V. R. Vittal, W. A. Bennett, and D. L. Tipton, "Development of an Advanced Vaneless Inlet Particle Separator for Helicopter Engines," *J Propul Power*, vol. 2, no. 5, pp. 438–444, Sep. 1986.
- [27] M. Taslim, A. Khanicheh, and S. Spring, "A Numerical Study of Sand Separation Applicable to Engine Inlet Particle Separator Systems," *Journal of the American Helicopter Society*, vol. 54, no. 4, pp. 42001–42001, 2009.
- [28] M. E. Taslim and S. Spring, "A Numerical Study of Sand Particle Distribution, Density, and Shape Effects on the Scavenge Efficiency of Engine Inlet Particle Separator Systems," *J. Am. Helicopter Society*, vol. 55, no. 2, p. 022006, 2010.
- [29] J. Wang, S. C. Kim, and D. Y. H. Pui, "Figure of merit of composite filters with micrometer and nanometer fibers," *Aerosol Science and Technology*, vol. 42, no. 9, pp. 722–728, 2008.